International Journal of Thermophysics (2024) 45:148
https://doi.org/10.1007/s10765-024-03431-2

Speed of Sound Measurements of Binary Mixtures of 1,1-Difluoroethylene (R-1132a) + Propane and Derived Speed of Sound of Pure R-1132a

Aaron J. Rowane[1] · **Richard A. Perkins**[1]

Received: 26 August 2024 / Accepted: 6 September 2024 / Published online: 16 October 2024

Abstract
Speed of sound data, measured using a dual-path pulse-echo instrument, are reported for three binary mixtures of 1,1-difluoroethylene (R-1132a) with propane at temperatures ranging from 230 to 345 K and pressures ranging from slightly above the bubble curve to a maximum pressure of 50 MPa. Significant attenuation of the pulse-echo signals was observed for measurements on pure R-1132a. Therefore, the R-1132a sample was doped with propane at mole fractions ranging from 0.0274 to 0.0887 and the propane + R-1132a mixture data was used to derive sound speeds for pure R-1132a. The data were compared to a preliminary equation of state for R-1132a, and deviations ranged from 2 % to 8 %. This demonstrates that the preliminary R-1132a EoS needs to be refit to better represent the speed of sound.

Keywords 1,1-Difluoroethylene · REFPROP · R-1132a · Speed of sound

1 Introduction

1,1-Difluoroethylene (R-1132a) has been identified as a low global warming potential (GWP) refrigerant of particular interest as a component in refrigerant blends used in ultra-low temperature (ULT) applications [1]. Present ULT refrigerants include the pure fluid trifluoromethane (R-23) and a blend of R-23 and hexafluoroethane (R-116)

Commercial equipment, instruments, or materials are identified only to adequately specify certain procedures. Such identification does not imply recommendation or endorsement by the National Institute of Standards and Technology, nor does it imply that the identified products are necessarily the best available for the purpose. Official contribution of the National Institute of Standards and Technology; not subject to copyright in the United States.

✉ Aaron J. Rowane
Aaron.Rowane@nist.gov

[1] Applied Chemicals and Materials Division, National Institute of Standards and Technology, Boulder, CO 80305, USA

referred to as R-508B. The 100-year GWP values for R-23 and R-116 are 12700 [2] and 13396, respectively. The 100-year GWP value for R-1132a is less than one and is therefore an attractive alternative to present ULT refrigerants. R-1132a has a molecular weight of 64.03 g·mol^{-1}, a critical temperature and pressure of 302.62 K, and 4.45 MPa [3], respectively, and triple point of 111.1 K [4]. R-1132a has a safety classification of A2 indicating that while it is non-toxic it is flammable [5]. The extremely low triple point of R-1132a supports its suitability as an ULT refrigerant.

Knowledge of the thermodynamic properties of refrigerants enables their efficient integration into refrigeration systems. Presently, several studies report thermodynamic data for R-1132a. Tomassetti and Di Nicola [6] report vapor pressure and vapor phase density data, Tomassetti et al. [4] report triple point data, Perera et al. [3] report *pvT* data and critical properties, Low [7] reports saturated liquid and vapor densities and heat capacities, Imai and co-workers [8] report surface tensions, and Demirdesen et al. [9] report vapor-phase speed of sound data. To the best of our knowledge, no liquid-phase speed of sound data has been reported in the literature for R-1132a. Liquid-phase speed of sound data are required to develop a robust reference equation of state (EoS) for R-1132a.

At the onset of this study, we attempted speed of sound measurements on pure R-1132a. However, significant attenuation of the pulse-echo signal was encountered due to the strong sound absorbing properties of R-1132a. This sound absorption resulted in weaker echo signals resulting in a lower signal-to-noise ratio, which can preclude speed of sound measurements. Therefore, in this study we applied a similar strategy to Lin and Trusler [10] who measured the speed of sound of carbon dioxide, which also exhibits strong sound absorption. The strategy of Lin and Trusler included both operating their instrument at a lower frequency and adding a small concentration of a doping agent to their sample to catalyze vibration–translation energy transfer in the fluid. In this study, to avoid impractical modifications of our instrument we only doped the R-1132a sample to overcome weak echo signals. As in the study of Lin and Trusler, propane was found to be a suitable doping agent for R-1132a. Measurements were performed for three R-1132a + propane mixtures at compositions ranging from 0.027 mole fraction to 0.089 mole fraction and the measured data obtained were used to derive sound speeds for pure R-1132a.

In 2020 Low [7] proposed a preliminary equation of state for R-1132a. The EoS was fit to saturated liquid isobaric heat capacities and saturated vapor and liquid density data. In the study by Low the isobaric heat capacity data was compared to the EoS with a root-mean-square deviations of 1.16 %. The isobaric heat capacity is a measure of how well an EoS represents derivative properties such as the speed of sound. An objective of the present study was to compare our sound speed data to the EoS of Low to evaluate its ability to represent derivative properties. Therefore, the data obtained in the present study was used to test the EoS of Low.

Table 1 Refrigerant samples used in this study listed with their CAS numbers, molar mass, source, and purity

Chemical name	CAS number	Molar mass ($g \cdot mol^{-1}$)	Source	Purity/mole percent
Propane	74–98-6	44.10	Scott specialty gases	99.999
1,1-difluoroethylene (R-1132a)	75–38-7	64.03	Koura	99.95

All samples were degassed using a freeze–pump–thaw method prior to preparing mixtures

Table 2 Mole fraction of propane in each mixture prepared (x_{C3}) listed with combined standard composition uncertainties ($u_c(x_{C3})$)

x_{C3}/mole fraction	$u_c(x_{C3})$/mole fraction
0.02737	0.00049
0.05075	0.00048
0.08868	0.00046

2 Materials and Methods

Table 1 lists the components used in this study with their IUPAC names, molar mass, source, and purity. As described in our previous studies [11, 12] degassed pure component samples were used to prepare vapor phase samples of each mixture. All mixtures were prepared gravimetrically using the double substitution weighing design of Harris [13]. The uncertainty in the mixture composition from gravimetric preparation was found to be less than 0.00005 mole fraction. Also considered in the composition uncertainty analysis were the impurities associated with the pure components used to prepare the mixture samples. Table 2 lists sample compositions, total sample masses, and combined expanded composition uncertainties for each mixture.

The dual-path pulse-echo instrument used to measure the speed of sound, sample preparation procedures, and loading procedures are identical to those described in previous studies and therefore are described elsewhere [11, 12, 14], and only the key differences in the measurement and pertinent information are restated here. It was found that the fluid of interest, R-1132a, like carbon dioxide [10], exhibits strong sound absorption that rendered speed of sound measurements of pure R-1132a impossible with the current dual-path pulse-echo instrument. Only a single short path echo was observed when loading R-1132a sample into the measuring cell. Lin and Trusler [10] describe two strategies to measure the speed of sound of strong sound absorbing molecules: (1) incorporate a lower frequency transducer into the instrument and (2) dope the sample with a suitable component to catalyze vibration–translation energy transfer in the fluid. In this study, it was not practical to make any modifications to the instrument. Therefore, the R-1132a sample was doped with propane at compositions ranging from approximately 0.027 mole fraction to 0.089 mole fraction and sufficiently strong echo signals were obtained to carry

out low uncertainty speed of sound measurements. Typically, for a single speed of sound measurement, we average 256 echoes, which provided a sufficient signal-to-noise ratio for sensitive measurements on most fluids. However, in this study up to 4096 echoes were averaged for each speed of sound measurement to increase the signal-to-noise ratio and acquire satisfactory echo data for analysis. A consideration with sound absorbing fluids when measuring the speed of sound is dispersion, which can result in an appreciable difference in the measured and thermodynamic speed of sound. Lin and Trusler, who used a 2 MHz transducer with a 50 mm path detection for a carbon dioxide/propane mixture, showed that the relative dispersion defined as $(c/c_0 - 1)$ was on the order of 10^{-4}. Similarly, in this study $(c/c_0 - 1)$ values were estimated to be on the order of 10^{-5} or less for all state points investigated. A detailed explanation on the dispersion calculations is included in the supplemental information (SI).

3 Experimental Results

Table 1 lists the measured temperature, pressure, and speed of sound, and the combined expanded uncertainty for each R-1132a/propane mixture. Measurements were performed along pseudo-isochores from 230 K to 345 K and pressures up to 50 MPa. The lower temperature and pressure limit was dictated by the strength and presence of both the short and long path echoes, which varied with the concentration of propane, temperature, and pressure. These data were averaged from up to twelve replicate speed of sound measurements at a given (T, p) state point. Data listing all of the unaveraged speed of sound measurements and their associated uncertainties can be found in the SI and in a data repository at nist.data.gov (https://doi.org/10.18434/mds2-3395).

Lin and Trusler [10] described an extrapolation procedure to derive speed of sound data for pure carbon dioxide from carbon dioxide/propane mixture data. Lin and Trusler performed speed of sound measurements along isotherms at several pressures for several carbon dioxide/propane mixtures. First, for each carbon dioxide/propane mixture, Lin and Trusler fit their isothermal speed of sound data to polynomial functions of pressure, $w(p)$. These polynomial functions were then used to calculate speed of sound values at equal pressures and temperatures for each carbon dioxide/propane composition. This enabled Lin and Trusler to fit the speed of sound to polynomials as a function of propane composition, $w(x_{C3})$. Extrapolating these polynomial functions of propane composition to zero mole fraction yielded speed of sound values for pure carbon dioxide.

Table 3 Experimental speed of sound data for the R-1132a/propane mixtures along pseudo-isochores

T/K	p/MPa	w/m·s^{-1}	$100 \cdot U_r(w)$
$x_{C3} = 0.02737$ ($u_c(x_{C3}) = 0.00049$)			
229.998	1.399	679.676	0.05
235.010	3.417	669.353	0.05
240.000	3.899	643.455	0.06
254.994	9.562	622.925	0.06
259.987	12.525	629.363	0.05
270.034	18.454	641.743	0.07
275.025	21.319	649.478	0.12
294.997	33.615	676.176	0.04
299.999	36.609	682.480	0.04
304.997	39.589	688.686	0.04
309.999	42.560	694.794	0.04
314.995	45.477	700.584	0.04
320.003	48.422	706.492	0.04
275.045	17.280	611.797	0.17
279.998	20.465	619.040	0.05
284.999	23.339	626.061	0.05
290.001	26.213	632.986	0.05
294.997	29.074	640.942	0.05
299.998	31.924	646.982	0.05
304.997	34.761	654.389	0.04
309.998	37.587	660.746	0.04
314.994	40.385	666.935	0.04
320.003	43.188	673.037	0.04
325.007	45.936	678.781	0.04
330.000	48.648	684.297	0.04
280.003	17.696	591.212	0.06
284.995	20.468	598.101	0.05
290.003	23.218	607.025	0.05
294.995	25.970	614.384	0.05
299.996	28.708	621.233	0.05
304.995	31.429	628.107	0.05
309.997	34.148	634.584	0.05
314.993	36.852	641.102	0.04
320.003	39.543	647.975	0.04
325.008	42.220	654.094	0.04
329.999	44.878	660.070	0.04
335.003	47.520	665.887	0.04
340.008	50.149	671.589	0.04
294.995	23.317	589.289	0.05
299.996	25.955	597.007	0.05

Table 3 (continued)

T/K	p/MPa	w/m·s^{-1}	$100 \cdot U_r(w)$
304.994	28.578	604.529	0.05
309.998	31.193	610.594	0.05
314.993	33.798	617.163	0.05
320.002	36.401	625.017	0.05
325.008	38.983	631.003	0.04
329.999	41.542	637.384	0.04
335.003	44.040	642.962	0.04
340.009	46.578	648.809	0.04
345.012	49.105	654.552	0.04
309.997	27.591	580.812	0.05
314.992	30.060	587.285	0.05
320.001	32.531	593.942	0.05
325.006	34.988	601.086	0.05
329.999	37.425	606.405	0.05
335.003	39.828	613.326	0.05
340.006	42.240	619.021	0.04
345.012	44.642	624.460	0.04
299.996	22.633	565.943	0.06
304.995	25.122	573.090	0.05
309.995	27.603	581.233	0.05
299.995	19.334	531.566	0.06
304.994	21.668	538.624	0.06
309.997	24.008	547.140	0.06
314.992	26.336	554.385	0.06
320.004	28.663	561.291	0.05
325.007	30.976	567.965	0.05
329.999	33.270	574.448	0.05
335.002	35.534	580.521	0.05
340.008	37.799	586.599	0.05
345.012	40.066	592.618	0.05
304.993	17.940	496.777	0.07
309.998	20.096	503.236	0.07
314.992	22.248	511.322	0.07
320.001	24.402	519.920	0.06
325.008	26.546	526.527	0.06
329.999	28.674	533.687	0.06
335.002	30.794	540.286	0.06
340.007	32.910	546.515	0.05
345.012	35.021	553.218	0.05
320.001	19.916	468.940	0.08
325.007	21.852	475.371	0.07

Table 3 (continued)

T/K	p/MPa	w/m·s^{-1}	$100 \cdot U_r(w)$
329.997	23.775	483.285	0.07
335.002	25.670	489.350	0.07
340.007	27.580	496.680	0.06
345.013	29.491	503.691	0.06
$x_{C3} = 0.05075$ ($u_c(x_{C3}) = 0.00048$)			
230.000	1.346	686.575	0.05
235.011	3.328	676.968	0.05
240.002	3.798	652.141	0.06
245.003	3.961	623.704	0.06
250.004	6.377	622.308	0.06
254.993	9.230	627.030	0.06
259.987	12.179	633.189	0.05
269.991	18.118	646.478	0.05
274.995	21.154	653.597	0.05
279.999	24.194	660.487	0.05
285.000	27.228	667.303	0.05
290.001	30.248	673.957	0.04
294.997	33.259	680.516	0.04
299.998	36.255	686.921	0.04
304.996	39.237	693.209	0.04
309.999	42.206	699.364	0.04
314.995	45.170	705.495	0.04
320.003	48.138	711.618	0.04
259.983	9.378	602.682	0.06
275.006	17.990	623.277	0.05
280.009	20.888	631.296	0.05
284.999	23.781	638.307	0.05
290.000	26.675	644.479	0.05
294.996	29.547	651.920	0.05
299.997	32.395	658.392	0.04
304.996	35.245	664.814	0.04
309.998	38.087	671.131	0.04
314.994	40.911	677.309	0.04
320.003	43.735	683.565	0.04
325.008	46.532	689.352	0.04
259.982	6.452	566.424	0.07
270.008	11.753	580.286	0.06
274.992	14.472	587.658	0.06
279.997	17.200	594.999	0.06
284.998	19.935	602.642	0.05
290.001	22.666	609.836	0.05
294.996	25.384	616.144	0.05

Table 3 (continued)

T/K	p/MPa	w/m·s^{-1}	$100 \cdot U_r(w)$
299.997	28.101	623.241	0.05
304.995	30.808	630.435	0.05
309.998	33.509	637.037	0.05
314.993	36.188	643.269	0.04
320.003	38.865	649.750	0.04
325.008	41.523	655.876	0.04
330.000	44.159	661.860	0.04
335.003	46.773	667.642	0.04
284.998	16.799	568.520	0.06
290.000	19.379	577.288	0.06
294.996	21.959	583.691	0.06
299.997	24.537	590.174	0.05
304.996	27.108	596.915	0.05
309.998	29.669	605.394	0.05
314.993	32.217	611.793	0.05
320.002	34.760	618.261	0.05
325.008	37.297	624.769	0.05
329.999	39.803	630.966	0.04
335.003	42.276	636.985	0.04
340.008	44.749	642.769	0.04
345.013	47.234	648.576	0.04
299.996	19.728	541.433	0.06
304.995	22.074	549.146	0.06
309.997	24.419	555.915	0.06
314.993	26.755	562.699	0.06
320.002	29.120	571.347	0.05
325.007	31.450	578.327	0.05
329.998	33.752	584.070	0.05
335.002	36.038	589.934	0.05
340.007	38.323	596.233	0.05
345.012	40.605	602.244	0.05
309.996	21.438	525.057	0.06
314.992	23.654	533.581	0.06
320.002	25.870	540.093	0.06
325.007	28.067	546.557	0.06
329.999	30.248	553.481	0.05
335.002	32.409	559.218	0.05
340.007	34.578	566.364	0.05
345.012	36.742	572.939	0.05
325.007	24.600	510.541	0.06
329.998	26.625	519.122	0.06

Table 3 (continued)

T/K	p/MPa	w/m·s^{-1}	$100 \cdot U_r(w)$
335.003	28.622	525.187	0.06
340.007	30.614	531.848	0.06
345.012	32.601	537.579	0.06
340.007	27.286	500.497	0.06
345.012	29.193	504.674	0.06
$x_{C3} = 0.08868$ ($u_c(x_{C3}) = 0.00046$)			
230.003	0.671	691.799	0.05
235.006	1.542	670.149	0.06
240.002	3.278	659.011	0.06
245.003	3.431	630.272	0.06
250.004	3.754	603.307	0.06
254.994	6.333	606.880	0.06
259.987	9.116	612.866	0.06
264.995	11.915	618.992	0.06
269.992	14.815	626.280	0.05
279.999	20.725	641.647	0.05
285.000	23.622	648.376	0.05
290.002	26.517	655.524	0.05
294.997	29.400	662.288	0.05
299.998	32.278	668.941	0.04
304.997	35.138	675.428	0.04
309.998	37.990	681.824	0.04
314.994	40.812	687.987	0.04
320.003	43.643	694.146	0.04
325.008	46.448	700.107	0.04
330.001	49.226	705.881	0.04
259.983	5.450	566.339	0.07
269.988	10.608	579.002	0.06
274.992	13.292	586.605	0.06
279.997	15.984	594.180	0.06
284.998	18.684	601.242	0.06
290.000	21.378	608.556	0.05
294.996	24.065	616.292	0.05
299.998	26.748	623.338	0.05
304.996	29.421	630.218	0.05
309.998	32.085	636.940	0.05
314.993	34.734	643.496	0.05
320.004	37.381	649.941	0.04
325.009	40.045	656.417	0.04
329.999	42.654	662.552	0.04
335.003	45.234	668.379	0.04

Table 3 (continued)

T/K	p/MPa	w/m·s^{-1}	$100 \cdot U_r(w)$
269.988	7.783	540.734	0.08
274.991	10.273	549.163	0.07
279.996	12.795	556.496	0.07
284.997	15.331	565.217	0.06
290.000	17.869	572.956	0.06
294.996	20.441	580.313	0.06
299.997	22.981	588.349	0.06
304.996	25.510	595.547	0.05
309.998	28.034	602.462	0.05
314.993	30.542	609.263	0.05
320.003	33.046	615.913	0.05
325.008	35.538	622.395	0.05
329.999	38.003	628.846	0.05
335.002	40.442	634.819	0.04
340.007	42.876	640.752	0.04
345.012	45.304	646.597	0.04
274.989	7.299	506.253	0.09
279.993	9.608	514.062	0.08
284.997	11.938	522.169	0.08
289.999	14.284	529.748	0.07
294.995	16.638	538.208	0.07
299.997	18.989	545.617	0.06
304.994	21.335	553.261	0.06
309.997	23.673	561.279	0.06
314.992	26.007	568.384	0.06
320.002	28.340	575.333	0.05
325.007	30.668	580.929	0.05
329.997	32.937	588.280	0.05
335.003	35.203	594.360	0.05
340.007	37.484	600.134	0.05
345.012	39.761	606.569	0.05
274.997	5.659	477.175	0.12
279.995	7.868	485.310	0.10
284.995	10.085	495.736	0.09
289.999	12.324	503.405	0.08
294.995	14.567	510.983	0.08
299.996	16.814	520.126	0.07
304.994	19.059	528.006	0.07
309.997	21.303	535.338	0.06
314.993	23.541	542.691	0.06
320.001	25.774	550.538	0.06

Table 3 (continued)

T/K	p/MPa	w/m·s^{-1}	$100 \cdot U_r(w)$
325.007	28.004	557.062	0.06
329.999	30.280	564.616	0.05
335.002	32.473	571.145	0.05
340.007	34.668	577.464	0.05
345.013	36.850	584.011	0.05
294.994	12.505	483.533	0.09
299.995	14.626	490.201	0.08
304.994	16.752	498.833	0.08
309.996	18.872	507.734	0.07
314.992	20.990	516.326	0.07
320.001	23.116	523.931	0.07
325.009	25.234	530.148	0.06
329.999	27.336	537.162	0.06
335.003	29.417	543.778	0.06
340.008	31.501	550.283	0.06
345.012	33.580	556.188	0.05
320.001	18.514	466.552	0.08
325.008	20.391	473.772	0.08
329.998	22.259	482.143	0.07
335.002	24.111	489.386	0.07
340.007	25.959	496.109	0.07
345.013	27.803	501.647	0.06
340.008	22.554	457.945	0.08
345.013	24.272	464.475	0.08

The different pseudo-isochores are separated by line breaks throughout the table. Speed of sound values listed are averaged from up to twelve replicate measurements at each state point. Compositions listed are mole fractions of propane (x_{C3}) along with their standard combined uncertainties ($u_c(x_{C3})$). $U_r(w)$ is the relative combined expanded uncertainty in the speed of sound determined with a coverage factor, $k = 2$

*The standard uncertainties for temperature and pressure are $u_c(T) = 0.004$ K and $u_c(p) = 0.014$ MPa, respectively

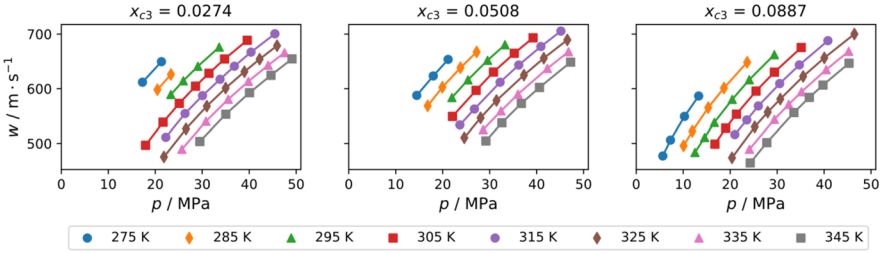

Fig. 1 Relationship between the sound speed and pressure for binary mixtures of R-1132a and propane where x_{C3} represents the mole fraction of propane in the mixture. Symbols represent experimental data points while lines are drawn are fitted polynomials. Only select isotherms are plotted to avoid clutter on the plot

The method of Lin and Trusler is applied here to determine the speed of sound of pure R-1132a with a few adjustments described herein. The data reported in our study were measured along pseudo isochores and not isotherms. Therefore, the first step in obtaining speed of sound values for pure R-1132a was to reorganize the pseudo-isochore data from Table 3 by temperature for each R-1132a/propane composition. The sound speeds in each isothermal grouping were not measured at even pressures. Figure 1 shows this reorganization of the speed of sound data along several nominal isotherms as a function of pressure for each R-1132a/propane mixture investigated. The isotherms were fit to first or second order polynomials in pressure depending on the number of data points obtained at a given temperature. For example, if only two data points were obtained at a given temperature, then the data was fit to a first order polynomial (linear function). If three data or more points were available, then the data was fitted to a second order polynomial. These fits of speed of sound as a function of pressure at each temperature and composition are then used to obtain "interpolated" values for the sound speed at even values of pressure.

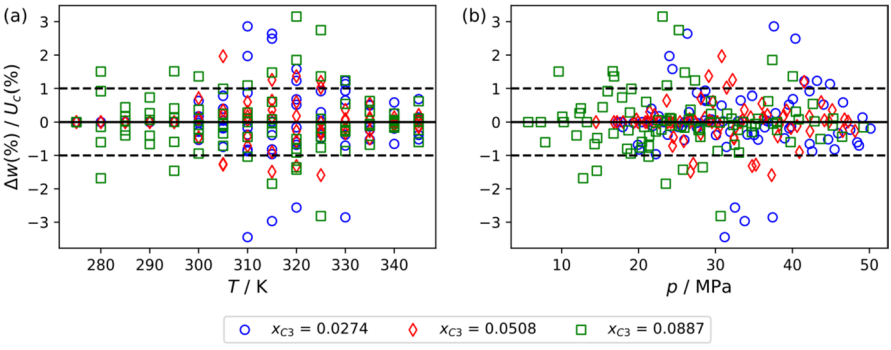

Fig. 2 Relationship between the ratio of the deviation of experimental speed of sound values, $\Delta w = 100 \cdot (w_{exp} - w_{calc})/w_{exp}$, where w_{exp} is an experimental speed of sound value and w_{calc} is calculated from the polynomial functions shown in Fig. 1, to the combined expanded uncertainty ($U_r(w)$) of the speed of sound measurement versus (a) temperature and (b) pressure

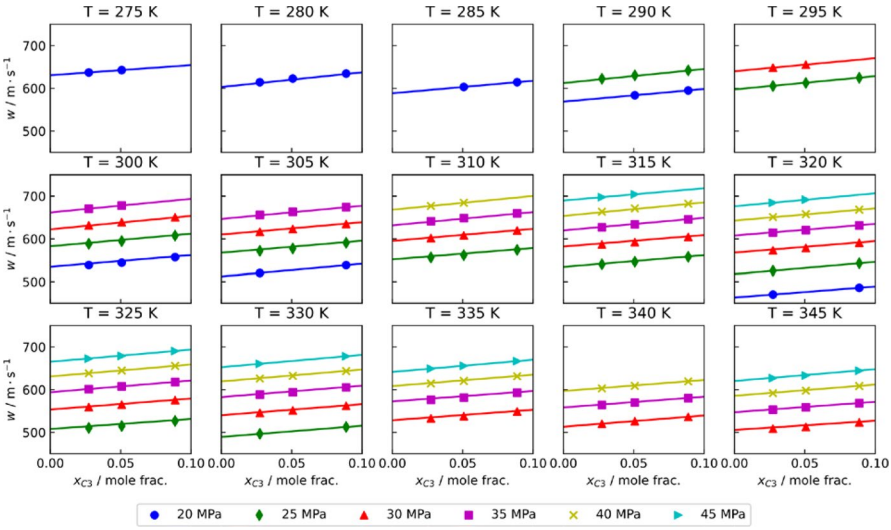

Fig. 3 Speed of sound isobars constructed from interpolated speed of sound data listed in Table 3 as a function of propane composition, x_{C3}

To discern the uncertainty contribution from this interpolation procedure, the performance of the polynomial functions in reproducing the speed of sound data must be known. Figure 2a and b show the relationship between the ratio of the deviation of experimental speed of sound values to those interpolated using polynomial fits of the isothermal data and the combined expanded experimental uncertainty of each data point listed in Table 3 versus temperature and pressure, respectively. Dashed lines drawn at 1 indicate that the deviations from the interpolation polynomials are within the estimated relative combined expanded uncertainty of the speed of sound measurements. The greatest deviations are seen between 305 K and 330 K at pressures below 40 MPa. It is important to note that the critical temperature and pressure of R-1132a are 302.81 K and 4.461 MPa, respectively [6]. This suggests that the data obtained between 305 K and 330 K may be in closer proximity to the mixture critical region for the R-1132a/propane blend where weaker echo signals are encountered resulting in underestimated uncertainties. 90 % of the data are within their estimated combined expanded experimental uncertainty with 95 % of the data within $1.5 \cdot U_r(w)$ of the experimental uncertainty. The average combined expanded uncertainty for all the data listed in Table 3 is 0.055 %. Given that 95 % of the data are within $1.5 \cdot U_r(w)$, we estimate the relative expanded uncertainty of the interpolated speed of sound values to be 0.083 % of the calculated value. This interpolation scheme provides a reasonable representation of the measured data given the challenges encountered with speed of sound measurements with weak echo signals.

Table 4 Derived 1,1-difluoroethylene (R-1132a) speed of sound values determined from the extrapolation of interpolated R-1132a/propane mixture data

T/K	p/MPa	w/m·s^{-1}	$100 \cdot U_r(w)$
275.000	20.000	630.67	0.09
280.000	20.000	603.05	0.08
285.000	20.000	588.44	0.09
290.000	20.000	568.79	0.09
290.000	25.000	612.41	0.08
295.000	25.000	597.47	0.08
295.000	30.000	640.02	0.10
300.000	20.000	534.75	0.08
300.000	25.000	582.78	0.08
300.000	30.000	622.37	0.08
300.000	35.000	661.82	0.09
305.000	20.000	512.32	0.10
305.000	25.000	567.74	0.08
305.000	30.000	610.16	0.08
305.000	35.000	646.7	0.08
310.000	25.000	552.09	0.08
310.000	30.000	595.26	0.08
310.000	35.000	631.65	0.08
310.000	40.000	668.23	0.09
315.000	25.000	534.4	0.08
315.000	30.000	582.15	0.08
315.000	35.000	619.87	0.08
315.000	40.000	653.77	0.08
315.000	45.000	689.74	0.09
320.000	20.000	463.12	0.11
320.000	25.000	517.77	0.10
320.000	30.000	568.01	0.08
320.000	35.000	607.83	0.08
320.000	40.000	642.8	0.08
320.000	45.000	676.31	0.10
325.000	25.000	508.07	0.08
325.000	30.000	553.51	0.08
325.000	35.000	594.09	0.08
325.000	40.000	630.99	0.08
325.000	45.000	665.34	0.08
330.000	25.000	489.43	0.10
330.000	30.000	540.31	0.08
330.000	35.000	582.73	0.08
330.000	40.000	619.33	0.08
330.000	45.000	652.65	0.10
335.000	30.000	528.51	0.08
335.000	35.000	572.61	0.08
335.000	40.000	608.58	0.08

Table 4 (continued)

T/K	p/MPa	w/m·s^{-1}	100·$U_r(w)$
335.000	45.000	641.63	0.08
340.000	30.000	513.31	0.08
340.000	35.000	558.44	0.08
340.000	40.000	596.86	0.08
345.000	30.000	505.83	0.08
345.000	35.000	547.37	0.08
345.000	40.000	585.73	0.08
345.000	45.000	620.42	0.08

$U_r(w)$ is the relative combined expanded uncertainty in the speed of sound determined with a coverage factor, $k=2$

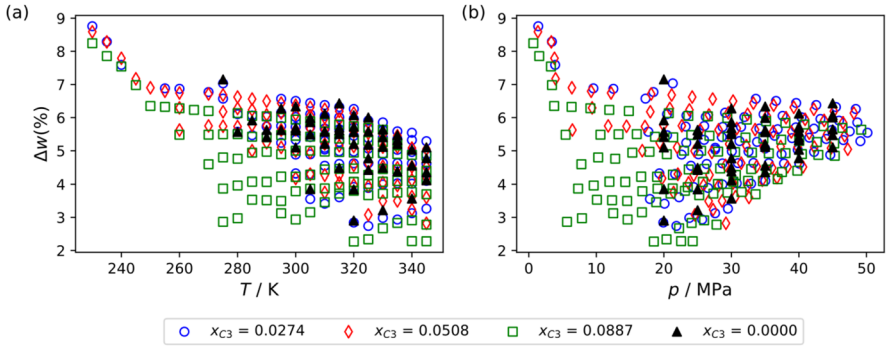

Fig. 4 Comparison the experimental speed of sound data reported in this study to the Helmholtz-energy-explicit equation of state. The Helmholtz-energy-explicit pure component EoS is reported by Lemmon et al. [15] for propane and the EoS of Low [7] for R-1132a. Symbols in comparisons versus (a) temperature and (b) pressure are for several propane compositions. The composition of 0.0000 is for pure R-1132a data extrapolated from R-1132a/propane mixture data

Table 5 Binary interaction parameters for the multifluid model estimated by REFPROP version 10.0[16]

Parameter	Value
β_T	1.00000
β_V	1.00000
γ_T	0.96645
γ_V	1.00590

The interpolation polynomials shown in Fig. 1 were used to obtain speed of sound values for each composition at the same even temperature and pressure. Figure 3 shows the relationship between the speed of sound and composition along several isobars at temperatures ranging from 275 K to 345 K at pressures ranging from 20 MPa to 45 MPa. Each of these isobars was fitted to either first or second order polynomials as a function of propane composition dependent on the number of data points available. By extrapolating each isobar to a propane

composition of 0 mole fraction, speed of sound values for pure R-1132a were obtained. Table 4 lists these derived R-1132a speed of sound values at temperatures ranging from 275 K to 345 K and pressures ranging from 18 MPa to 45 MPa. Data below 275 K are not considered here since sufficient data at all three compositions were not available to construct isobars without extrapolation of isothermal data sets. The expanded uncertainty listed in Table 4 was estimated by adding, in quadrature, the error in the intercept of the fit to each isobar and the standard uncertainty in the speed of sound values interpolated from the polynomials in Fig. 1 and then applying a coverage factor, $k = 2$.

4 Discussion

Figure 4a and b are deviation graphs comparing the R-1132a/propane mixture data and derived R-1132a speed of sound data to the most recent Helmholtz-energy-explicit equation of state. The pure fluid equations of state used for propane is reported by Lemmon et al. [15] and R-1132a from Low [7]. No binary interaction parameters were available for the R-1132a/propane mixture, and thus parameters estimated by REFPROP version 10.0 [16] were used. The binary interaction parameters estimated by REFPROP are listed in Table 5. The average absolute deviation (Δ_{AAD}), defined by Eq. 1, is 5.1 % with a maximum deviation of 8.8 % when including both the R-1132a/propane mixture data and R-1132a data derived from R-1132a/propane mixture data. It is important to note that no liquid-phase speed of sound data was used to develop the R-1132a pure fluid EoS.

5 Conclusions

Weak echo signals were encountered when attempting speed of sound measurements on pure R-1132a. Thus, the R-1132a sample was doped with propane at varying compositions ranging from 0.02737 mole fraction to 0.08868 mole fraction to catalyze vibration-translation energy transfer in the fluid. Analogous to previous experiments by Lin and Trusler [10] for carbon dioxide, propane was found to be a suitable doping agent for R-1132a to catalyze vibration-translation energy transfer to increase the echo signal strength. The speed of sound was measured for three R-1132a+propane binary mixtures, and the resultant data was used to derive speed of sound data for pure R-1132a. The experimental speed of sound data for both R-1132a/propane mixtures and derived for pure R-1132a deviate from 2 % to 10 % from mixture models incorporating the pure fluid EoS of Lemmon et al. [15] and the EoS of Low [7] for R-1132a using binary interaction parameters estimated by REFPROP version 10.0 [16]. Deviations were found to be consistent across all three R-1132a/propane mixtures samples and the derived R-1132a speed of sound data. Given that the pure fluid EoS of Lemmon et al. for propane has an estimated relative uncertainty of 0.03 % for speed of sound at temperatures ranging from 260 K to 420 K it is anticipated that the significant R-1132a deviations are a result of deficiencies in the R-1132a pure fluid EoS. The data reported in the present study can be used

to develop a more reliable EoS for R-1132a, which would be capable of accurately depicting the speed of sound as well as other important derivative properties.

6 Supplementary Material

Included in the supplemental information is a ZIP folder containing the unaveraged speed of sound data and a description of the procedure used to determine the impact of dispersion on the speed of sound measurements.

Supplementary Information The online version contains supplementary material available at https://doi.org/10.1007/s10765-024-03431-2.

Acknowledgments We thank Stephanie Outcalt for degassing the pure R-1132a sample, and Mark McLinden for his guidance in preparing the gas mixtures for the speed of sound measurements and technical discussions pertinent to this work. We gratefully acknowledge the support of the U.S. Department of Energy, Building Technologies Office under Agreement 892434-19-S-EE000031.

Author's Contributions A.J.R. Performed the measurements, prepared the samples, correlated the data, compared to the models, generated the figures, and wrote the main manuscript. R.A.P. analyzed the data and edited the main manuscript.

Funding Open access funding provided by the National Institutes of Health. This work was funded by the U.S. Department of Energy, Building Technologies Office under Agreement 892434-19-S-EE000031.

Data Availability The data reported in this study are deposited at nist.data.gov (DOI: https://doi.org/10.18434/mds2-3395).

Declarations

Conflict of interests The authors declare no competing interests.

References

1. A. Mota-Babiloni, A. Fernández-Moreno, P. Giménez-Prades, C.-M. Udroiu, J. Navarro-Esbrí, Int. J. Refrig. **148**, 108 (2023). https://doi.org/10.1016/j.ijrefrig.2023.01.006
2. G. Myhre, D. Shindell, Climate Change 2013 *The Physical Science Basis*: Chapter 8 Anthropogenic and Natural Radiative Forcing. (2014)
3. U. Perera, K. Miyane, N. Sakoda, K. Thu, Y. Higashi, Int. J. Thermophys. **44**, 84 (2023) . https://doi.org/10.1007/s10765-023-03184-4
4. S. Tomassetti, G. Di Nicola, C. Kondou, Int. J. Refrig. **133**, 172 (2022). https://doi.org/10.1016/j.ijrefrig.2021.10.008

5. P. Giménez-Prades, J. Navarro-Esbrí, C. Arpagaus, A. Fernández-Moreno, A. Mota-Babiloni, Renew. Sustain. Energy Rev. **167**, 112549 (2022). https://doi.org/10.1016/j.rser.2022.112549
6. S. Tomassetti, G. Di Nicola, Fluid Phase Equilib. **533**, 112939 (2021) https://doi.org/10.1016/j.fluid.2021.112939
7. R. Low, 1st IIR international conference on the application of HFO refrigerants, Birmingham, United Kingdom (2018) . https://doi.org/10.18462/IIR.HFO.2018.1183
8. T. Imai, T. Kawahara, R. Nonaka, S. Tomassetti, T. Okumura, Y. Higashi, G. Di Nicola, C. Kondou, J. Mol. Liq. **407**, 125262 (2024). https://doi.org/10.1016/j.molliq.2024.125262
9. D. Demirdesen, C. Wedler, R.E. Low, J.P.M. Trusler, Int. J. Thermophys. **44**, 90 (2023). https://doi.org/10.1007/s10765-023-03198-y
10. C.-W. Lin, J.P.M. Trusler, J. Chem. Eng. Data **59**, 4099 (2014). https://doi.org/10.1021/je5007407
11. A.J. Rowane, R.A. Perkins, Int. J. Thermophys. **43**, 46 (2022). https://doi.org/10.1007/s10765-021-02966-y
12. A.J. Rowane, R.A. Perkins, J. Chem. Eng. Data **67**, 1365 (2022). https://doi.org/10.1021/acs.jced.2c00037
13. G.L. Harris, Selected laboratory and measurement practices and procedures to support basic mass calibrations. NISTIR 6969 edn. (National Institute of Standards and Technology, 2003)
14. M.O. McLinden, R.A. Perkins, Ind. Eng. Chem. Res. **62**, 12381 (2023). https://doi.org/10.1021/acs.iecr.3c01720
15. E.W. Lemmon, M.O. McLinden, W. Wagner, J. Chem. Eng. Data **54**, 3141 (2009). https://doi.org/10.1021/je900217v
16. E.W. Lemmon, I.H. Bell, M.L. Huber, M.O. McLinden, NIST Standard Reference Database 23: Reference Fluid Thermodynamic and Transport Properties-REFPROP, version 10.0 (Gaithersburg, 2018)